

1 **Estimating Transient Climate Response in a large-ensemble global climate model simulation**

2

3 B.K. Adams and A.E. Dessler*

4 Dept. of Atmospheric Sciences, Texas A&M University, College Station, TX

5 * corresponding author, adessler@tamu.edu

6

7 Main points:

8 1. In a large model ensemble, we find that estimates of TCR from the 20th century tends to
9 be low biased compared to the model's true TCR.

10 2. Internal variability can push down or enhance the warming in ensemble members &
11 lead to large errors in TCR inferred from the 20th century.

12 3. We also verify that the details of the construction of the temperature dataset from
13 which TCR is inferred can lead to significant biases in TCR inferred from observed
14 warming.

15

16 **Plain language summary:**

17 The transient climate response (TCR) is defined to be the warming after 70 years of a 1% per
18 year increase in atmospheric CO₂. It is one of the important metrics in climate science because
19 it plays a key role in determining how much warming we will experience in the future. Previous
20 work has found that TCR inferred from observed warming over the 20th century tends to be
21 lower than TCR in climate models. This has been used by suggest that climate models are
22 overpredicting future warming. We use a large number of climate model runs to investigate
23 the methodology of this comparison. We find that TCR estimated from the 20th century
24 simulations may indeed be much lower than the model's true TCR. This arises from biases in
25 the methodology of estimating TCR from 20th century warming, as well as biases in the
26 construction of the observational temperature data sets. We therefore find no evidence that
27 models are overestimating TCR.

28

29 Abstract

30 The transient climate response (TCR), defined to be the warming in near-surface air
31 temperature after 70 years of a 1% per year increase in CO₂, can be estimated from observed
32 warming over the 19th and 20th centuries. Such analyses yield lower values than TCR estimated
33 from global climate models (GCMs). This disagreement has been used to suggest that GCMs'
34 climate may be too sensitive to increases in CO₂. Here we critically evaluate the methodology
35 of the comparison using a large ensemble of a fully coupled GCM simulating the historical
36 period, 1850–2005. We find that TCR estimated from model simulations of the historical period
37 can be much lower than the model's true TCR, replicating the disagreement seen between
38 observations and GCM estimates of TCR. This suggests that the disagreement could be
39 explained entirely by the methodology of the comparison and undercuts the suggestions that
40 GCMs overestimate TCR.

41 Introduction

42 The transient climate response (TCR) is frequently used to quantify the sensitivity of our climate
43 system to increases in greenhouse gases. It is defined to be the warming in near-surface air
44 temperature after 70 years of a 1% per year increase in atmospheric CO₂. As described below,
45 it can be estimated from observed warming over the 19th and 20th centuries, yielding most-
46 likely TCR values of 1.3-1.6 K [Bengtsson and Schwartz, 2013; Otto et al., 2013; Richardson et
47 al., 2016; Lewis and Curry, 2018]. These values lie below the CMIP5 ensemble average TCR of
48 1.8 K [Forster *et al.*, 2013]. Resolving this disagreement may have important consequences for
49 our confidence in the fidelity of climate models and their simulations of future climate change.

50 We will test the methodology of this comparison using a large model ensemble, an increasingly
51 popular tool to study the impact of internal variability on the climate system. The most
52 appropriate ensemble for this type of problem contains many runs of a single model with
53 identical physics and external forcing but different initial conditions, which allows one to infer
54 the impact of internal variability in the absence of inter-model differences. As each ensemble
55 member evolves in time, internal variability of the different members is out of phase, leading to
56 differences in the climate states among the ensemble members. In fact, one can think of our

57 observational record as one member of a theoretical ensemble of Earth’s climate trajectories.
58 A model ensemble therefore gives us insight into what alternative climate histories may have
59 looked like.

60 **Data**

61 We analyze output from an ensemble of 100 runs of the fully-coupled Max Planck Institute
62 Earth System Model version 1.1 (MPI-ESM1.1) covering the period 1850-2005. The ensemble
63 was used by Dessler et al. [2018] to characterize the impact of internal variability on estimates
64 of the equilibrium climate sensitivity (ECS); they found that internal variability can lead to
65 significant errors in ECS inferred from historical observations. Hedemann et al. [2017] analyzed
66 this ensemble to determine potential causes of the so-called warming hiatus that occurred in
67 the 2000s.

68 As described by Dessler et al. [2018]: “This is the latest coupled climate model from the Max
69 Planck Institute for Meteorology and consists of the ECHAM6.3 atmosphere and land model
70 coupled to the MPI-OM ocean model. The atmospheric resolution is T63 spectral truncation,
71 corresponding to about 200 km, with 47 vertical levels, whereas the ocean has a nominal
72 resolution of about 1.5 degrees and 40 vertical levels. MPI-ESM1.1 is a bug-fixed and improved
73 version of the MPI-ESM used during CMIP5 [Giorgetta *et al.*, 2013] and nearly identical to the
74 MPI-ESM1.2 ... model being used to provide output to CMIP6, except that the historical forcings
75 are from the MPI-ESM. Each of the 100 members simulates the years 1850-2005 (Fig. 1) and
76 use the same evolution of historical natural and anthropogenic forcings. The members differ
77 only in their initial conditions —each starts from a different state sampled from a 2000-year
78 control simulation.”

79 Dessler et al. further say: “We calculate effective radiative forcing F for the ensemble by
80 subtracting top-of-atmosphere flux R in a run with climatological sea surface temperatures
81 (SSTs) and a constant pre-industrial atmosphere from average R from an ensemble of three
82 runs using the same SSTs but the time-varying atmospheric composition used in the historical
83 runs [Hansen *et al.*, 2005; Forster *et al.*, 2016]. The three-member ensemble begins with
84 perturbed atmospheric states.”

85 We estimate $F_{2\times\text{CO}_2}$ using the same approach in a set of fixed SST runs, one with a pre-industrial
 86 atmosphere and one in which CO_2 increases at 1% per year. $F_{2\times\text{CO}_2}$ is then estimated as the
 87 average difference in top-of-atmosphere flux over years 62-78, which produces a value of 3.7
 88 W/m^2 . This is lower than the value used in Dessler et al. [2018], 3.9 W/m^2 , which was
 89 estimated as one-half of the $4\times\text{CO}_2$ forcing from the same runs. Because of the slight non-
 90 linearity in the relation between forcing and the logarithm of CO_2 , taking one half of the $4\times\text{CO}_2$
 91 forcing is an overestimate of $F_{2\times\text{CO}_2}$.

92 We also analyze a 68-member ensemble of the MPI-ESM1.1 forced with CO_2 increasing at
 93 1%/year (hereafter, “1% runs”). As with the historical ensemble, the 1% ensemble members
 94 differ only in their initial conditions — each starts from a different state sampled from a 2000-
 95 year pre-industrial control simulation.

96 **Analysis of biases in TCR**

97 Time series of global-average near-surface air temperature for all 100 members are plotted in
 98 Fig. 1 of Dessler et al. [2018]; that plot shows that the model ensemble is in good agreement
 99 with observed surface temperatures. TCR can be estimated from the ensemble’s temperature
 100 data with this equation [Gregory and Forster, 2008; Otto *et al.*, 2013; Richardson *et al.*, 2016]:

$$101 \quad \text{TCR}_{hist} = \Delta T \frac{F_{2\times\text{CO}_2}}{\Delta F} \quad (1)$$

102 where ΔT is the change in temperature over the historical period and ΔF is the change in
 103 radiative forcing. In our analysis, Δ represents the change between the 1859-1882 average,
 104 selected because it is not strongly influenced by volcanic eruptions [Mauritsen and Pincus,
 105 2017; Lewis and Curry, 2018], and the average of the last ten years of the runs, 1996-2005. We
 106 refer to TCRs estimated this way as TCR_{hist} .

107 We first calculate TCR_{hist} in each ensemble member using global-average near-surface air
 108 temperature for ΔT . The calculated values range from 1.32 to 1.94 K (5-95% range 1.48-1.90 K)
 109 (Fig. 1a, Table 1). The spread in these TCR estimates is entirely due to internal variability and
 110 the spread is similar to previous estimates [Huber *et al.*, 2014; Hawkins *et al.*, 2016]. The

111 standard deviation of ΔT from the ensemble is 0.07 K, close to that assumed by Lewis and Curry
112 [2015], implying a similar spread in TCR due to internal variability in their analysis.

113 TCR is formally defined as the warming of global-average near-surface air temperature in
114 response to CO_2 increasing at 1% per year, at the time of doubling. This value, which we will
115 call TCR_{true} , can be estimated by averaging the warming (relative to pre-industrial) in years 60-
116 80 of the 68-member ensemble of 1% runs. We find that TCR_{true} for the MPI-ESM1.1 is 1.78 K;
117 this is 0.10 K (5.8%) larger than the average of the ensemble's TCR_{hist} (1.68 K).

118 Thus, TCR_{hist} is a low-biased estimate of TCR_{true} in the ensemble. The magnitude, and even the
119 sign, of this bias varies depending on the portion of the historical record being examined (Table
120 1). Overall, though, we see a clear tendency for the TCR_{hist} to underestimate TCR_{true} . Previous
121 papers have suggested that the biases in TCR_{hist} could be due to aerosol forcing efficacy
122 [Kummer and Dessler, 2014; Shindell, 2014; Marvel *et al.*, 2015], although that explanation
123 remains to be validated in this ensemble.

124 We are now in a position to critically evaluate previous comparisons of TCR from observations
125 and GCMs. TCR estimated from observations, which are TCR_{hist} , have most-likely values in the
126 range 1.3-1.6 K [Bengtsson and Schwartz, 2013; Otto *et al.*, 2013; Richardson *et al.*, 2016; Lewis
127 and Curry, 2018], although the uncertainty in the individual estimates is large. The CMIP5
128 ensemble's TCR, which are TCR_{true} , fall in the range 1.8 ± 0.6 K (average and 5-95% confidence
129 interval) [Forster *et al.*, 2013]. Our analysis of the MPI-ESM1.1 ensemble demonstrates how a
130 model with a TCR_{true} of 1.78 K might nevertheless produce TCR_{hist} in some ensemble members
131 that that are much lower (1.3-1.4, Figure 1a) and in agreement with observational estimates.

132 We can also confirm previous suggestions that two issues with the observed ΔT , masking and
133 blending, are further biasing TCR_{hist} to even lower values [Richardson *et al.*, 2016]. Masking
134 refers to the fact that the observations are geographically incomplete, and that the degree of
135 incompleteness has changed over time, leading to biases in global-average ΔT [Cowtan and
136 Way, 2014]. To test the impact of this on TCR_{hist} , we also calculated ΔT in the ensemble using a
137 time-varying mask derived from HadCRUT4 (v4.6.0.0) [Morice *et al.*, 2012]. Using this masked
138 ΔT in Eq. 1, ensemble average TCR_{hist} drops from 1.68 K to 1.59 K (Fig. 1b, Table 2). However,

139 this masking bias is bigger in some observational data sets than others. If we mask the
140 ensemble's temperatures following the Berkeley Earth gridded land-ocean data set [Rohde *et*
141 *al.*, 2013] we find a much smaller bias (Table 2).

142 The second issue is blending, which refers to the fact that observed ΔT data sets are usually a
143 blend of near-surface air temperature over land and sea ice but sea surface temperature (SST)
144 over open ocean. Because near-surface air temperature is warming faster than SSTs, this
145 blending lowers ΔT compared to an estimate derived entirely from near-surface air
146 temperature [Cowtan *et al.*, 2015; Santer *et al.*, 2000]. We test this by calculating a blended ΔT
147 in the ensemble, which we also mask following HadCRUT4. Using this blended and masked ΔT ,
148 ensemble average TCR_{hist} drops to 1.47 K (Fig. 1d, Table 2). Masking with Berkeley Earth again
149 provides a less-biased estimate, with ensemble average TCR_{hist} of 1.55 K (Table 2).

150 In these blending calculations, we calculate anomalies of the individual data sets first, and then
151 combine them. We have also blended absolute temperatures and then calculated anomalies;
152 we find that the order of calculation changes our results by less than 1% [Cowtan *et al.*, 2015].
153 Finally, we have also calculated blended ΔT using the temperature of the model's top ocean
154 layer (representing the top 12 m of the ocean) instead of SST. Using that estimate of ΔT yields
155 TCR_{hist} estimates that are similar to those that blend SST (Fig. 2f, Table 2).

156 **Analysis of internal variability in the ensemble**

157 The wildcard in this analysis is internal variability. Given that we have only one realization of the
158 historical record, there is no way for us to know whether the warming over the historical period
159 is less or greater than the average trajectory of our climate system over the historical period.
160 Any deviation of the observed record from the "ensemble average" of the Earth's historical
161 climate trajectory would lead directly to biases in TCR_{hist} estimated from observations. Our
162 analysis shows that this variability could explain the vast majority of the difference in TCR
163 between observations and models.

164 The global and ensemble average ΔT is 0.84 K over the historical period, in good agreement
165 with observational estimates. The spatial distribution of ensemble-average ΔT (Fig. 2) shows
166 largest warming in the Arctic and least warming in the Southern Ocean (55°S), which is

167 consistent with the observed pattern of warming over this time. The tropics (30°N-30°S) are
168 responsible for 44% of the ensemble-average warming, the northern hemisphere extratropics
169 (30°N-90°N) is responsible for 39%, and the southern hemisphere extratropics (30°S-90°S) is
170 responsible for the rest, 17%.

171 The pattern of surface warming varies among the members of the ensemble, which is what
172 drives differences in the TCR. We can visualize this by plotting the covariance between the
173 ensemble's 100 TCR values and the ensemble's 100 ΔT values at each grid point (Fig. 3). Most
174 regions show positive covariances, meaning higher TCRs are associated with more warming
175 almost everywhere.

176 But the covariance is not uniform — the spread in TCR arises mainly from ΔT variability in the
177 northern hemisphere: 54% of the global average covariance comes from the northern
178 hemisphere extratropics, 34% from the tropics (30°N-30°S), and 12% from the southern
179 hemisphere extratropics. Previous work has shown that, for equilibrium climate sensitivity, the
180 southern hemisphere plays the dominant role in variability in the ensemble [Dessler *et al.*,
181 2018].

182 High values of covariance in the northern hemisphere extratropics are found in the Arctic,
183 especially the Barents Sea, as well as Northern Europe and the North Atlantic. The main
184 contribution in the southern hemisphere extratropics is in the Weddell Sea, just to the east of
185 the Antarctic Peninsula. Previous researchers have identified these regions as playing key roles
186 in internal variability [Brown *et al.*, 2016; Martin *et al.*, 2013]. We are presently performing a
187 more detailed analysis of the causes of internal variability in the ensemble that will be
188 published in a future paper.

189 **Conclusions**

190 We have investigated why observation-based estimates of TCR tend to be lower than those
191 from GCMs using a perfect model experiment. We have quantified a number of biases that can
192 explain most, perhaps even all, of the disagreement: 1) a bias between TCR_{hist} and TCR_{true} , 2) a
193 bias due to incomplete spatial coverage in the observational ΔT record, and 3) a bias due to the
194 observational ΔT values being blends of air temperature and SSTs. These three biases are all

195 acting in the same direction, to push TCR_{hist} to lower values. The impact of internal variability,
196 which can suppress warming in some members of the ensemble, thereby further reducing
197 TCR_{hist} , has a potentially large magnitude and therefore could also be playing a major role in the
198 model-observation difference.

199 The uncertainty in individual estimates of TCR_{hist} from observations are large and the
200 uncertainty range easily covers most of the TCR_{true} values from the CMIP5 ensemble [Lewis and
201 Curry, 2015; Lewis and Curry, 2018; Richardson *et al.*, 2016]. Because of the large uncertainty
202 in other parameters (e.g., aerosol forcing), adding uncertainty due to the issues we discuss in
203 this paper will produce only nominal increases in the total uncertainty of the observational
204 estimates. However, the biases we have investigated are capable of explaining the entire
205 disagreement between the central values of the estimates, which has been the focus of much
206 of the discussion.

207 Our work also informs how future analyses should be done. First, analyses should account for
208 the role of internal variability, most likely by comparing observations to an ensemble of runs. In
209 addition, we should not compare TCR_{hist} derived from observations to TCR_{true} — unless one can
210 quantify and adjust for the bias between these methods. A better approach would be to
211 compare TCR_{hist} from observations to TCR_{hist} derived from an ensemble of runs of the GCMs
212 covering the same period as the observations. Finally, one must account for biases in the
213 observations of ΔT due to masking and blending, most likely by calculating masked and blended
214 ΔT fields from the model and using those to estimate the model-derived TCR_{hist} .

215

216 **Acknowledgments:** This work was supported by NSF grant AGS-1661861 to Texas A&M
217 University. We thank the Bjorn Stevens, Thorsten Mauritsen, and Chris Hedemann of the Max-
218 Planck-Institut für Meteorologie for their help interpreting output from the ensemble that
219 formed the basis of this analysis. We also thank Mark Richardson for his suggestions on the
220 manuscript. Data and code are available from TBD.

221

222 **References**

- 223 Bengtsson, L., & S. E. Schwartz (2013), Determination of a lower bound on Earth's climate
224 sensitivity, *Tellus B: Chemical and Physical Meteorology*, 65, 21533, doi:
225 10.3402/tellusb.v65i0.21533.
- 226 Brown, P. T., W. Li, J. H. Jiang, & H. Su (2016), Spread in the magnitude of climate model
227 interdecadal global temperature variability traced to disagreements over high-latitude
228 oceans, *Geophys. Res. Lett.*, 43, 12,543-512,549, doi: 10.1002/2016GL071442.
- 229 Cowtan, K., & R. G. Way (2014), Coverage bias in the HadCRUT4 temperature series and its
230 impact on recent temperature trends, *Q. J. R. Meteor. Soc.*, 140, 1935-1944, doi:
231 doi:10.1002/qj.2297.
- 232 Cowtan, K., Z. Hausfather, E. Hawkins, P. Jacobs, M. E. Mann, S. K. Miller, et al. (2015),
233 Robust comparison of climate models with observations using blended land air and
234 ocean sea surface temperatures, *Geophys. Res. Lett.*, 42, 6526-6534, doi:
235 10.1002/2015GL064888.
- 236 Dessler, A. E., T. Mauritsen, & B. Stevens (2018), The influence of internal variability on
237 Earth's energy balance framework and implications for estimating climate sensitivity,
238 *Atmos. Chem. Phys.*, 18, 5147-5155, doi: 10.5194/acp-18-5147-2018.
- 239 Forster, P. M., T. Andrews, P. Good, J. M. Gregory, L. S. Jackson, & M. Zelinka (2013),
240 Evaluating adjusted forcing and model spread for historical and future scenarios in the
241 CMIP5 generation of climate models, *Journal of Geophysical Research: Atmospheres*,
242 118, 1139-1150, doi: 10.1002/jgrd.50174.
- 243 Forster, P. M., T. Richardson, A. C. Maycock, C. J. Smith, B. H. Samset, G. Myhre, et al. (2016),
244 Recommendations for diagnosing effective radiative forcing from climate models for
245 CMIP6, *J. Geophys. Res.*, 121, 12460-12475, doi: 10.1002/2016jd025320.
- 246 Giorgetta, M. A., J. Jungclaus, C. H. Reick, S. Legutke, J. Bader, M. Böttinger, et al. (2013),
247 Climate and carbon cycle changes from 1850 to 2100 in MPI-ESM simulations for the
248 Coupled Model Intercomparison Project phase 5, *Journal of Advances in Modeling Earth
249 Systems*, 5, 572-597, doi: 10.1002/jame.20038.
- 250 Gregory, J. M., & P. M. Forster (2008), Transient climate response estimated from radiative
251 forcing and observed temperature change, *J. Geophys. Res.*, 113, doi:
252 10.1029/2008jd010405.
- 253 Hansen, J., M. Sato, R. Ruedy, L. Nazarenko, A. Lacis, G. A. Schmidt, et al. (2005), Efficacy of
254 climate forcings, *Journal of Geophysical Research: Atmospheres*, 110, doi:
255 10.1029/2005JD005776.
- 256 Hawkins, E., R. S. Smith, J. M. Gregory, & D. A. Stainforth (2016), Irreducible uncertainty in
257 near-term climate projections, *Climate Dynamics*, 46, 3807-3819, doi: 10.1007/s00382-
258 015-2806-8.
- 259 Hedemann, C., T. Mauritsen, J. Jungclaus, & J. Marotzke (2017), The subtle origins of
260 surface-warming hiatuses, *Nature Clim. Change*, 7, 336-339, doi:
261 10.1038/nclimate3274.

- 262 Huber, M., U. Beyerle, & R. Knutti (2014), Estimating climate sensitivity and future
263 temperature in the presence of natural climate variability, *Geophys. Res. Lett.*, 41, 2086-
264 2092, doi: 10.1002/2013GL058532.
- 265 Kummer, J. R., & A. E. Dessler (2014), The impact of forcing efficacy on the equilibrium
266 climate sensitivity, *Geophys. Res. Lett.*, 41, 3565-3568, doi: 10.1002/2014gl060046.
- 267 Lewis, N., & J. A. Curry (2015), The implications for climate sensitivity of AR5 forcing and
268 heat uptake estimates, *Climate Dynamics*, 45, 1009-1023, doi: 10.1007/s00382-014-
269 2342-y.
- 270 Lewis, N., & J. Curry (2018), The impact of recent forcing and ocean heat uptake data on
271 estimates of climate sensitivity, *J. Climate*, doi: 10.1175/jcli-d-17-0667.1.
- 272 Martin, T., W. Park, & M. Latif (2013), Multi-centennial variability controlled by Southern
273 Ocean convection in the Kiel Climate Model, *Climate Dynamics*, 40, 2005-2022, doi:
274 10.1007/s00382-012-1586-7.
- 275 Marvel, K., G. A. Schmidt, R. L. Miller, & L. S. Nazarenko (2015), Implications for climate
276 sensitivity from the response to individual forcings, *Nature Climate Change*, 6, 386, doi:
277 10.1038/nclimate2888.
- 278 Mauritsen, T., & R. Pincus (2017), Committed warming inferred from observations, *Nature*
279 *Climate Change*, 7, 652-655, doi: 10.1038/nclimate3357.
- 280 Morice, C. P., J. J. Kennedy, N. A. Rayner, & P. D. Jones (2012), Quantifying uncertainties in
281 global and regional temperature change using an ensemble of observational estimates:
282 The HadCRUT4 data set, *J. Geophys. Res.*, 117, doi: 10.1029/2011jd017187.
- 283 Otto, A., F. E. L. Otto, O. Boucher, J. Church, G. Hegerl, P. M. Forster, et al. (2013), Energy
284 budget constraints on climate response, *Nature Geoscience*, 6, 415-416, doi:
285 10.1038/ngeo1836.
- 286 Richardson, M., K. Cowtan, E. Hawkins, & M. B. Stolpe (2016), Reconciled climate response
287 estimates from climate models and the energy budget of Earth, *Nature Clim. Change*, 6,
288 931-935, doi: 10.1038/nclimate3066.
- 289 Rohde, R., R. A. Muller, R. Jacobsen, E. Muller, S. Perlmutter, A. Rosenfeld, et al. (2013), A
290 new estimate of the average earth surface land temperature spanning 1753 to 2011,
291 *Geoinfor. Geostat.: An Overview*, 1, doi: 10.4172/2327-4581.1000101.
- 292 Santer, B. D., T. M. L. Wigley, D. J. Gaffen, L. Bengtsson, C. Doutriaux, J. S. Boyle, et al. (2000),
293 Interpreting differential temperature trends at the surface and in the lower
294 troposphere, *Science*, 287, 1227.
- 295 Shindell, D. T. (2014), Inhomogeneous forcing and transient climate sensitivity, *Nature*
296 *Climate Change*, 4, 274, doi: 10.1038/nclimate2136.
- 297

298

299

Table 1. TCR_{hist} calculated with different base and end periods

base period	end period	average (K)	Full TCR range (K)	5-95% TCR range (K)	width (K)	% diff from true TCR	ΔF (W/m^2)
1859-1882	1940-1949	1.82	0.63-2.88	1.15-2.50	1.35	2.0	0.54
1859-1882	1951-1960	1.96	1.10-3.13	1.32-2.67	1.34	9.2	0.59
1859-1882	1969-1978	1.71	1.01-2.91	1.24-2.24	0.99	-4.0	0.81
1859-1882	1996-2005	1.68	1.32-1.94	1.48-1.90	0.42	-5.9	1.85
1930-1939	1996-2005	1.65	0.97-2.07	1.35-1.99	0.64	-7.9	1.41
1940-1949	1996-2005	1.62	1.02-2.16	1.28-2.04	0.76	-9.6	1.31
1951-1960	1996-2005	1.55	0.91-2.04	1.20-1.90	0.70	-14.8	1.26
1970-1979	1996-2005	1.67	0.99-2.42	1.20-2.09	0.90	-6.6	0.99

300 The bold line is the case primarily discussed in the text. Width is the difference between the 5th and 95th
 301 percentile values; % difference is average TCR_{hist} minus TCR_{true} , 1.78 K, divided by average TCR_{hist} , in
 302 percent; ΔF is the change in forcing between the base and end periods.

303

304

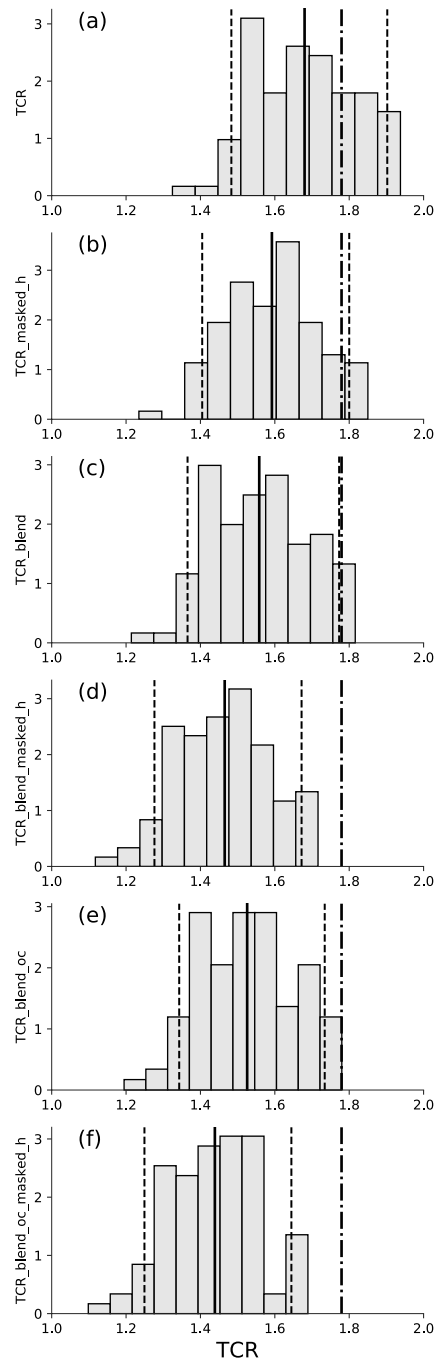
305 **Table 2. TCR_{hist} calculated with different versions of ΔT**

Ts data set	Description	average (K)	% diff from True TCR	Full TCR range (K)	5-95% TCR range (K)
TCR	ΔT is global-average near-surface air temperature	1.68	-5.9	1.32-1.94	1.48-1.90
TCR_masked_h	Same as TCR, but geographic coverage follows HadCRUT4	1.59	-11.8	1.23-1.85	1.40-1.80
TCR_masked_b	Same as TCR, but geographic coverage follows Berkeley Earth	1.67	-6.5	1.30-1.93	1.48-1.89
TCR_blend	ΔT is a blend of near-surface air temperature over land and sea ice and SSTs over open ocean	1.56	-14.2	1.21-1.82	1.37-1.77
TCR_blend_masked_h	Same as TCR_blend, but geographic coverage follows HadCRUT4	1.47	-21.4	1.12-1.72	1.28-1.67
TCR_blend_masked_b	Same as TCR_blend, but geographic coverage follows Berkeley Earth	1.55	-14.7	1.19-1.80	1.36-1.77
TCR_blend_oc	ΔT is a blend of near-surface air temperature over land and sea ice; elsewhere, use temperature of the top 12 m of the ocean	1.53	-16.6	1.19-1.78	1.34-1.73
TCR_blend_oc_masked_h	Same as TCR_blend_oc, but geographic coverage follows HadCRUT4	1.44	-23.7	1.10-1.69	1.25-1.64
TCR_blend_oc_masked_b	Same as TCR_blend_oc, but geographic coverage follows Berkeley Earth	1.51	-17.7	1.17-1.76	1.33-1.73

306 The bold line is the base case primarily discussed in the text; % difference is average TCR_{hist} minus
307 TCR_{true} , 1.78 K, divided by average TCR_{hist} , in percent.

308

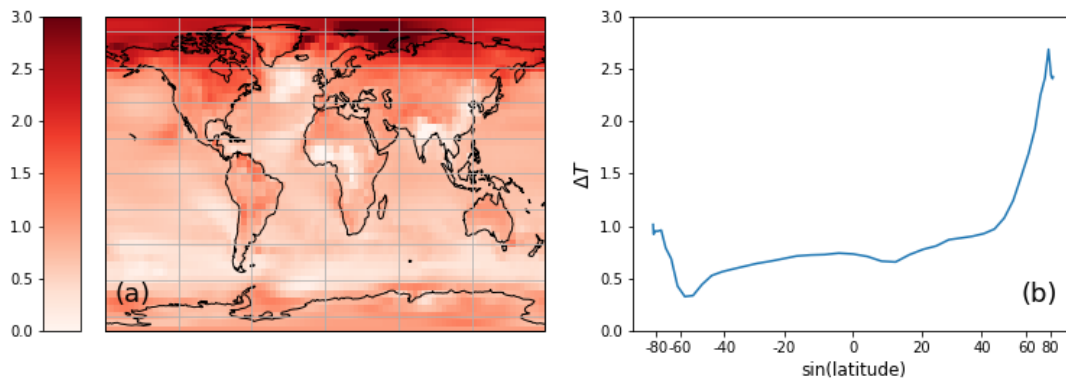
309



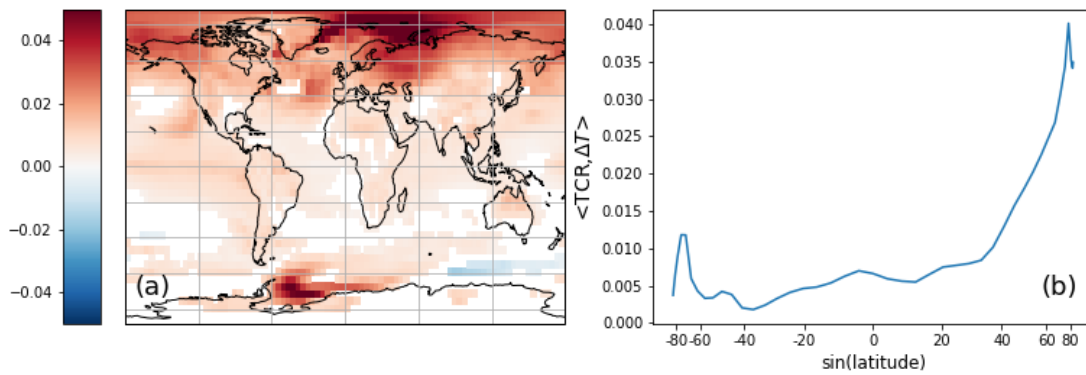
310

311

312 Figure 1. Histograms of TCR_{hist} (K) from the ensemble. Each panel shows the calculation with a
 313 different version of ΔT ; see Table 2 for definitions. The solid black line represents the average,
 314 the dashed lines are the 5th and 95th percentiles. The dot-dashed line is TCR_{true} of the model,
 315 1.78 K.



316
 317 Figure 2. (a) Spatial distribution of ensemble average ΔT (K), the average change in temperature
 318 between 1859-1882 and 1996-2005; (b) zonal average ΔT (K) vs. area-weighted latitude.
 319



320
 321 Figure 3. (a) Covariance of the ensemble's TCR and each grid point's ΔT (K^2); regions where the
 322 covariance is not statistically different from zero (5-95% confidence interval, estimated by a
 323 bootstrap technique) are white. (b) Covariance of TCR and zonal average ΔT (K^2).
 324